Adsorption Energetics of Amino-Acid Analogs on Polymer/Water Interfaces Studied by All-Atom Molecular Dynamics Simulation and a Theory of Solutions

Nobuhiro Yasoshima,[†] Tatsuya Ishiyama,[‡] and Nobuyuki Matubayasi[*,†]

[†]*Division of Chemical Engineering, Graduate School of Engineering Science, Osaka University, Toyonaka, Osaka 560-8531, Japan*

[‡]*Department of Applied Chemistry, Graduate School of Science and Engineering, University of Toyama, Toyama 930-8555, Japan*

E-mail: nobuyuki@cheng.es.osaka-u.ac.jp

Abstract

Energetics of adsorption was addressed with all-atom molecular dynamics simulation on the interfaces of poly(2-methoxyethyl acrylate) (PMEA), poly(methyl methacrylate) (PMMA), and poly(butyl acrylate) (PBA) with water. A wide variety of adsorbate solutes were examined, and the free energy of adsorption was computed with the method of energy representation. It was found that the adsorption free energy was favorable (negative) for all the combinations of solute and polymer, and among PMEA, PMMA, and PBA, the strongest adsorption was observed on PMMA for the hydrophobic solutes and on PMEA for the hydrophilic ones. According to the decomposition of the adsorption free energy into the contributions from polymer and water, it was seen that the polymer contribution is larger in magnitude with the solute size. The total free energy of adsorption was correlated well with the solvation free energy in bulk water only for hydrophobic solutes. The roles of the intermolecular interaction components such as electrostatic, van der Waals, and excluded-volume were further studied, and the electrostatic component was influential only to determine the polymer dependences of the adsorption capacities of hydrophilic solutes. The extent of adsorption was shown to be ranked by the van der Waals component in the solute-polymer interaction separately over the hydrophilic and hydrophobic solutes, with the excluded-volume effect from water pointed out to also drive the adsorption.

INTRODUCTION

Adsorption on an interface with water is an important factor determining surface properties of a polymer, such as blood compatibility in medical devices and low fouling in separation membranes. The capacity of adsorption depends strongly on the chemical structure of the polymer, and a guideline connecting the polymer structure and the adsorption capacity needs to be sought. The adsorption capacity of a polymer has recently been analyzed in terms of its interaction with water. This is based on the idea that water around the adsorption site needs to be displaced when the adsorbate is transferred to the interface.[1–7] It should be noted that the extent of adsorption is

actually determined by the cooperation and/or competition of intermolecular interactions among the polymer, water, and adsorbate molecules. The specific nature of an adsorbate is reflected in its interactions with the polymer and water, and toward quantitative assessment of the adsorption capacity, the interactions of the adsorbate as well as those between the polymer and water[8,9] are preferably treated at atomic resolution.

In this work, we develop an atomistic approach to the free energy of adsorption onto a polymer/water interface. The extent of adsorption is quantified at the thermodynamic level by the free energy of adsorption, which is the free-energy change for bringing the adsorbate molecule from bulk liquid to the interface with the polymer. Upon adsorption onto the interface with water, the adsorbate-water interaction is (partially) lost and the adsorbate-polymer interaction emerges. Explicit treatment of both interactions is thus important to reveal the interaction component that governs the capacity and specificity of adsorption. The roles of the adsorbate-polymer and adsorbate-water interactions are not readily separated in experimental approaches, though. Molecular dynamics simulation (MD) is advantageous to analyze the intermolecular interactions in connection to the structures of the adsorbate and polymer at atomic resolution. The present work focuses on the adsorption free energies of a series of hydrophobic and hydrophilic molecules using all-atom MD and free-energy calculations.

The polymers examined are poly(2-methoxyethyl acrylate) (PMEA), poly(methyl methacrylate) (PMMA), and poly(butyl acrylate) (PBA). PMEA is known to be a biocompatible polymer, and with the diffuse distribution of hydrophilic moieties, it denatures adsorbed proteins to lesser extents than other polymers.[10,11] PMMA is a widely used polymer with a hydrophobic methyl group bonded directly to the main chain. PBA has a more hydrophobic side chain than PMEA, while the chain mobility is estimated to be similar according to the glass-transition temperatures.[12] The adsorbate molecules examined are amino-acid analogs. They are building blocks of proteins and are studied to provide a basis for understanding the adsorption capacities of biomolecules. A wide range of interactions from the hydrophobic to hydrophilic can be studied by employing the amino-acid analogs, and the thermodynamics of hydration was indeed studied intensively, for ex-

ample, by Wolfenden et al.'s measurements of the hydration free energies.[13] In the present work, we compute the adsorption free energies of analog adsorbates onto the polymer/water interfaces. We characterize how the hydrophobicity and hydrophilicity of an analog adsorbate are reflected in the extent of adsorption and analyze the roles of intermolecular interaction components such as electrostatic and van der Waals in adsorption energetics. The interaction of water at the interfaces with bioinert polymers was actually stressed in previous works.[10,12] In our free-energy analysis, we quantify the separated contributions from polymer and water and show the importance of the van der Waals interaction between the solute and polymer.

The adsorption free energy is the free energy of transfer from the liquid bulk to the polymer surface and may be calculated with such a standard method as umbrella sampling.[14,15] This type of calculation is of much demand especially for polymer systems, however, since a number of intermediate configurations need to be introduced to describe the approach of the adsorbed molecule to the surface and the structural relaxation is usually slow for polymer. In the present work, we circumvent the use of intermediate states and employ a theory of solutions to determine the adsorption free energy. According to a thermodynamic cycle, the adsorption process of an adsorbate molecule from the bulk liquid onto the polymer surface can be decomposed into the transfers from the bulk liquid to vacuum and from vacuum to the adsorption site of interest. The former transfer is the reverse process of solvation in the bulk liquid, and the free-energy change associated with it is the solvation free energy. The latter may also be treated as a solvation by viewing the adsorbate molecule as the solute and the polymer and water as the solvent. The solvation free energy is then the free-energy change for turning on the intermolecular interactions between the solute and solvent thus identified, with a condition that the solute is restrained at the adsorption site. In this treatment, the solvent consists of two species and is inhomogeneous due to the presence of polymer/water interface, and to compute the free energy of solvation in an inhomogeneous, mixed-solvent system, we adopt the method of energy representation. It is a distribution-function theory of solutions and provides the solvation free energy through a functional formulated in terms of distribution functions of the solute-solvent pair interaction energy.[16–19] In the energy-representation

method, the molecular simulation of the polymer-water system is to be conducted only for the state without the solute and the one with the adsorbed solute. No simulation is necessary for the intermediate configurations that describe the approach of the solute from liquid bulk to the polymer surface, leading to the reduction of computational load. Among a variety of approximate methods of free energy,[20–33] the energy-representation method is unique in compromising the accuracy and efficiency with applicability to molecules with intramolecular degrees of freedom as well as to interfaces.[34–46] It was previously applied to bulk polymers and to air/water and solid/water interfaces, and good agreements with numerically exact results were reported for the adsorption of a urea molecule at the interface between urea crystal and liquid water over a wide variety of adsorption configurations.[37,38,42,43,46]

In our approach, the polymer and water are treated as a mixed solvent and the solute adsorbate is subject to the intermolecular interactions with the two solvent species. It is then of interest to separate the contributions from the respective solvent species. The separated contributions are not observable in general, though, and a model of solvation needs to be employed to conduct the separation. The free-energy functional in the energy-representation formalism offers a framework meeting this necessity. The functional is formally expressed as a sum of the contributions from the respective solvent species and allows the decomposition of the adsorption free energy into the contributions from the polymer and water. We discuss the cooperation and/or competition of the effects of the polymer and water within the framework of the energy-representation formalism.

METHODS

The structures of the polymers examined in the present work are shown in Figure 1. Each polymer species was atactic at a meso-diad ratio of 0.5 as generated by J-OCTA,[47] and the degree of polymerization N was 80 for each polymer. The polymer/water systems were also analyzed at N = 40, and Figure S1 shows that the interfacial structures are insensitive to N. The adsorbate solutes were amino-acid side-chain analogs listed in Table 1.[13,36,39,48] Cyclic glycylglycine peptide

(diketopiperazine) was also adopted as a model solute for the backbone, and the energetic values for the backbone analog were taken to be halves of the corresponding values for cyclic glycyl-glycine peptide.[39,49,50] The general Amber force field (GAFF)[51] was employed for the polymers and amino-acid analog solutes, and the TIP3P model[52] was used for water. The atomic charges were determined by RESP (restrained electrostatic potential),[53] as described in Appendix A.

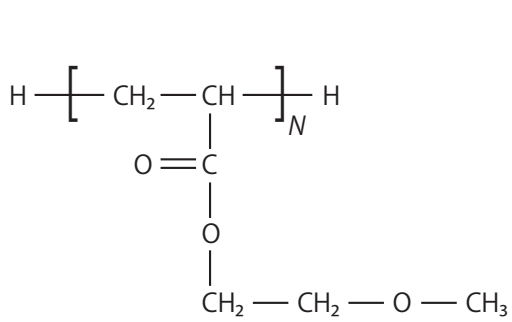

poly(2-methoxyethyl acrylate) (PMEA)

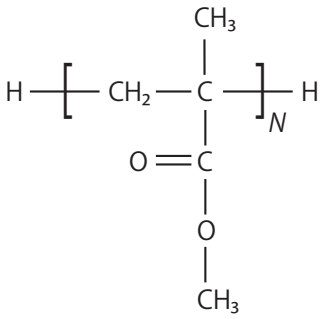

poly(methyl methacrylate) (PMMA)

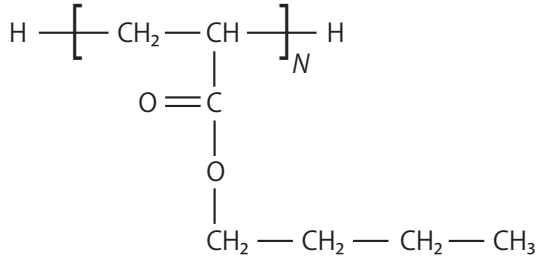

poly(*n*-butyl acrylate) (PBA)

Figure 1: Polymers examined in the present work.

All the simulations were conducted using GROMACS 2021.3.[54] The periodic boundary condition was employed with the minimum image convention, and the number of polymer molecules in the unit cell of MD was 16, 20, and 16 for PMEA, PMMA, and PBA, respectively, when $N = 80$ and was doubled for each polymer at $N = 40$. The smooth particle-mesh Ewald (PME) method[55,56] was utilized to handle the electrostatic interaction with a real-space cutoff of 1.2 nm, a spline order

Table 1: Correspondence of the amino-acid side chains to their analogs.

Amino acid	Analog solute	Amino acid	Analog solute	Amino acid	Analog solute
Ala	methane	Val	propane	Leu	iso-butane
Ile	n-butane	Met	methyl ethyl sulfide	Cys	methanethiol
Ser	methanol	Thr	ethanol	Asn	acetamide
Gln	propionamide	Tyr	p-cresol	Trp	3-methylindole

of 4, and a Fourier grid spacing of 0.12 nm for each of the x, y, and z directions. The Lennard-Jones (LJ) interaction was combined with the Lorentz-Berthelot rule for unlike pairs of atoms and was truncated at 1.2 nm by applying the switching function operative in a range of 1.0-1.2 nm.[57] The long-range correction of the LJ interaction was not carried out, given that the polymer/water systems examined in the present work are inhomogeneous.

The simulation was conducted through the steps in Table 2. At the start of step 1, the polymer molecules with the same structures that had been generated by J-OCTA[47] as noted at the beginning of this section were located with PACKMOL[58] randomly in the MD unit cell at a density of 0.006 g/cm^3 with the number of polymer molecules described in the preceding paragraph. The unit cell was cubic at steps 1-3, and was deformed to the rectangular form of x:y:z = 3:3:1 at step 4. At the beginning of step 7, a vacuum region of 8 nm was added along the z direction both above and below the polymer cell obtained at the end of step 6. When step 10 was started, each of the upper (more positive z) and lower (more negative z) regions of the polymer slab was filled with 6000 water molecules. In both the polymer/vacuum and polymer/water systems, the interface was planar and spanned over the x and y directions with the z direction normal to the interface. Accordingly, two interfaces were involved in the system and the total number of water molecules in the MD unit cell was 12000 for the polymer/water system. The system was annealed at steps 6 and 8. In the former, the relaxation of the polymer structure was facilitated at high temperature and pressure, and in the latter, the interface was relaxed by gradual reduction of the temperature. After the equilibration,

the production was done at 300 K and 1 bar for 2 ns at a sampling interval of 1 ps.

The leap-frog stochastic dynamics method[59,60] was adopted to integrate the equation of motion at the time step listed in Table 2 and regulate the temperature at an inverse friction constant of 1 ps. The pressure was maintained with the Parrinello-Rahman barostat[61] at a time constant of 1 ps with an isothermal compressibility of 4.5×10^{-5} bar^{-1}. The pressure coupling was isotropic at steps 1-9 and semi-isotropic for the lateral (x and y) and normal (z) directions at the following steps. The LINCS (LINear Constraint Solver) algorithm[62] was employed for the polymers and amino-acid analogs to fix the bond lengths involving a hydrogen atom, and SETTLE[63] was used to keep the water molecules rigid.

Table 2: Simulation steps

step	run[a]	simulation time (ns)	temperature (K)	pressure (bar)	MD time step (fs)	
polymer bulk						
1	EM					
2	NVT	0.5	300		0.5	
3	NPT	5	300	1	2	
4	NVT	1	300		2	Deformed from x:y:z = 1:1:1 to 3:3:1
5	NPT	1	300	1	2	
6[b]	NPT	4	2000 $\rightleftarrows$ 300	1000 $\rightleftarrows$ 1	0.5 $\rightleftarrows$ 2	MD was performed twice at each of the 2000 K and 300 K states.
polymer/vacuum interface						
7	NVT	1	300		2	
8	NVT	20	500 $\rightarrow$ 300		2	Gradual reduction of temperature at 10 K ns^{-1}
9	NVT	1	300		2	
polymer/water interface						
10	EM					
11	NVT	0.5	300		0.5	
12	NPT	1	300	1	2	
13	NVT	1	300		2	
only for the solution system containing an analog solute						
14	EM					
15	NVT	0.5	300		0.5	Set the charge of the solute to 0
16	NVT	1	300		2	
production run						
17	NVT	2	300	1	2	

[a] EM stands for the energy minimization done with the method of steepest descent to a maximum force of 25 kcal mol^{-1} Å^{-1}, and NVT and NPT mean the MD simulations in the NVT and NPT ensembles, respectively.

[b] MD was performed in the order of (2000 K, 1000 bar) $\rightarrow$ (300 K, 1 bar) $\rightarrow$ (2000 K, 1000 bar) $\rightarrow$ (300 K, 1 bar), and each was run for 1 ns. The time step of MD was 0.5 and 2 fs at 2000 K and 300 K states, respectively.

As will be described in the next paragraph, the simulated system involved a single solute molecule or did not contain any solute molecule. Steps 14-16 were performed only for the former kind of system and were skipped in the latter. At step 14, the solute was placed with random orientation by setting its center of mass to the Gibbs dividing surface for the polymer slab along the z direction and a random position along x and y. The charges on the atomic sites of the solute were set to 0 at step 15 to turn off strong forces due to electrostatic interactions of the inserted solute with polymer and water molecules. The solute molecule was further subject to a restraint expressed as

$$\frac{1}{2}k(z-d)^2H(z-d) \tag{1}$$

at steps 15-17 of Table 2, where z is the distance along the z direction of the solute center of mass from the Gibbs dividing surface, k is the force constant, H is the Heaviside step function, and the restraint was operative only when $z > d$. The restraint was implemented to keep the solute at the polymer/water interface, and k and d were 1000 kcal mol^{-1}Å^{-2} and 5 Å, respectively.

The adsorption free energy of an amino-acid analog solute was computed as the difference between the transfer free energy of the solute from vacuum to the polymer/water interface and that from vacuum to the liquid bulk. These free energies of transfer were calculated with the method of energy representation, and in the case of interface, the adsorbed molecule was treated as the solute and the polymer and water molecules as solvent species. The "solvation" is then the change of the state from the "reference solvent" consisting only of polymer and water to the "solution" system of interest that involves the solute molecule at the interface. The "solvation free energy" $\Delta\mu$ corresponds to the free-energy change of turning on the intermolecular interactions between the (mixed) solvent and the solute molecule placed at the polymer/water interface, and to compute $\Delta\mu$ with the energy-representation method, MD simulations were conducted for the solution system, for the reference solvent, and for the isolated solute located in vacuum. The force fields were the same among the three systems, and the simulation setups were identical between the solution and reference-solvent systems except for those related to the solute. The isolated solute is an amino-acid analog in vacuum, and an isothermal MD simulation of the single solute was carried out for

10 ns with a sampling interval of 0.1 ps. The electrostatic potential was then set to its bare form of $1/r$ without cutoff, and the LJ interaction was handled with the same procedure as that for the solution and reference-solvent systems. To obtain $\Delta\mu$ through the energy-representation method, the configuration of the solution system was counted only when the center-of-mass position of the solute is within ± 5 Å from the Gibbs dividing surface. Correspondingly, the solute sampled in vacuum was inserted as a test particle into the reference-solvent system within ± 5 Å position for the solute center of mass from the Gibbs dividing surface at random orientation. The number of test-particle insertions was 100 per reference-solvent configuration sampled, and 2×10^5 solute-solvent configurations were generated in total for a single reference-solvent run. Actually, the simulation procedures in Table 2 were repeated 60 and 30 times for the solution and reference solvent, respectively.[43,46,64–68] The ensemble averages were then obtained from the total production times of 120 and 60 ns, respectively, and the approximate functional for $\Delta\mu$ is provided in ref 40.

The solvation free energy $\Delta\mu$ was also calculated in bulk water. In this case, the MD cell was cubic and the number of water molecules contained in it was 6000. The solution system had one solute molecule, in addition, and its production was carried out for 1 ns with a sampling interval of 0.1 ps. The reference solvent was pure water with a simulation time of 0.5 ns, and was sampled every 0.1 ps. The solute was inserted 500 times at random position and orientation against each solvent configuration sampled. The other simulation setups were identical to those described above for the polymer/water system, and the free energy of adsorption was obtained as the difference of the $\Delta\mu$ at the interface from the $\Delta\mu$ in bulk water.

RESULTS AND DISCUSSION

We first study the interfacial structures of the polymer/water systems without adsorbate solutes. The direction normal to the interface is taken to be z, and $z = 0$ is the center of mass of the polymer molecules in each system examined. Figure 2 shows the density profiles of polymer and water expressed with the masses of all the atoms. The average density of the polymer in the inner

region of -1.0 nm $< z <$ 1.0 nm is 1172, 1080, and 1015 kg m^{-3} for PMEA, PMMA, and PBA, respectively, and they agree with the corresponding, experimental values within 9%. The polymer and water densities vary over a spatial range of $\sim$2 nm. The thickness of the interface can be quantified by the 10-90 thickness, which is defined as the difference between the z coordinates at which the density of the polymer is 10% and 90% of the value within the inner region quoted above. Actually, there are two interfaces in the positive and negative z regions in our simulations, and the 10-90 thickness noted here is the average of the two values evaluated in the positive and negative z. The 10-90 thickness is 1.05, 1.25, and 0.94 nm for PMEA, PMMA, and PBA, respectively. The interface is the sharpest for PBA, and the water density in the interfacial region is also the smallest for PBA among the polymer/water systems examined. A purely hydrophobic moiety is present in the side chain of PBA, indeed, leading to the lesser extent of water penetration into the polymer region. For the polymer/vacuum interface, the 10-90 thickness was 0.90, 1.26, and 0.90 nm for PMEA, PMMA, and PBA, respectively. The interface expands with water for the polymer with more hydrophilic side chains, such as PMEA.[69]

As noted in METHODS section, MD simulations were performed also at the degree of polymerization $N = 40$. The results with $N = 40$ are provided in Figure S1, and it is seen that the average density of the polymer computed in the inner region of the polymer slab of -1.0 nm $< z <$ 1.0 nm agrees between $N = 40$ and 80 within 0.8%. The 10-90 thickness was also in agreement within 0.15 nm.

The free energy of adsorption $\Delta\mu^{\mathrm{ad}}$ was determined as the difference between the transfer free energy of the solute from vacuum to the interface and that from vacuum to the water bulk. Figure 3(a) shows $\Delta\mu^{\mathrm{ad}}$ onto the interfaces of PMEA, PMMA, and PBA with water. $\Delta\mu^{\mathrm{ad}}$ is favorable (negative) for all the combinations of solute and polymer, and the amino-acid analogs are located favorably on the polymer/water interface. Figure 3(d) also shows the solvation free energy of each solute in bulk water $\Delta\mu^{\mathrm{bulk}}$ as a reference. This is the transfer free energy from vacuum to water and is a measure of the hydrophobicity and hydrophilicity of the solute. It has been shown actually that the $\Delta\mu^{\mathrm{bulk}}$ values calculated in previous studies are in agreement with

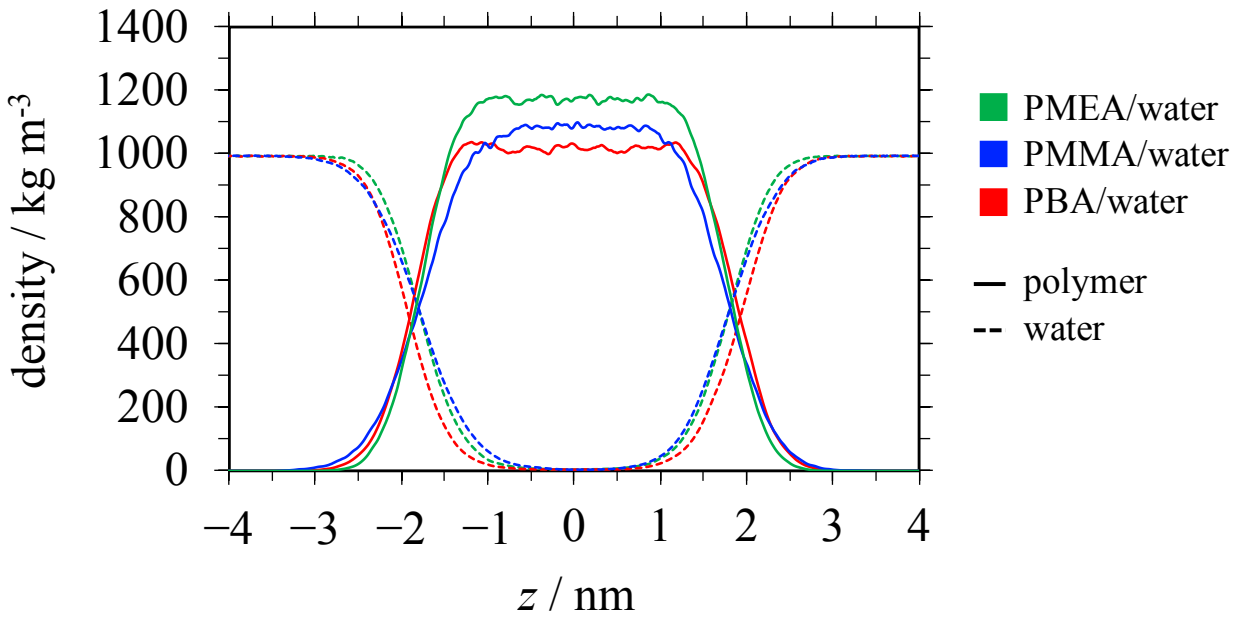

Figure 2: Density profiles of the polymer/water systems. The abscissa z is taken to be the distance along the direction normal to the interface, and its zero is set to the center of mass of the polymer molecules. The densities are expressed with respect to the masses of all the atoms including the hydrogens.

the experimental ones and the numerically exact results from the Bennett acceptance ratio (BAR) method.[13,39,48] According to Table 1, the Ala, Val, Leu, and Ile analogs are hydrocarbons, and in the following, they will be called hydrophobic solutes. The Ser, Thr, Asn, Gln, Tyr, Trp, and backbone analogs have favorable (negative) $\Delta\mu^{\mathrm{bulk}}$ in Figure 3(d) and will be noted as hydrophilic. Met and Cys are between the hydrophobic and hydrophilic species with respect to $\Delta\mu^{\mathrm{bulk}}$ and will be referred to as sulfur-containing solutes. Among the hydrocarbon solutes of the Ala, Val, Leu, and Ile analogs, $\Delta\mu^{\mathrm{ad}}$ becomes more favorable with the number of carbon atoms. The strength of adsorption of the hydrophobic solute correlates to its size. The magnitudes of $\Delta\mu^{\mathrm{ad}}$ for those four solutes are larger on the PMMA/water interface than on PMEA and PBA, furthermore. PMMA has short side chains, and with the methyl group bonded to the main chain, it adsorbs the hydrophobic solutes most strongly. $\Delta\mu^{\mathrm{ad}}$ will also be decomposed into the polymer and water contributions later with respect to Figures 3(b) and 3(c), and the polymer contribution leads to PMEA $>$ PBA for the adsorption strengths for the Val, Leu, and Ile analogs.

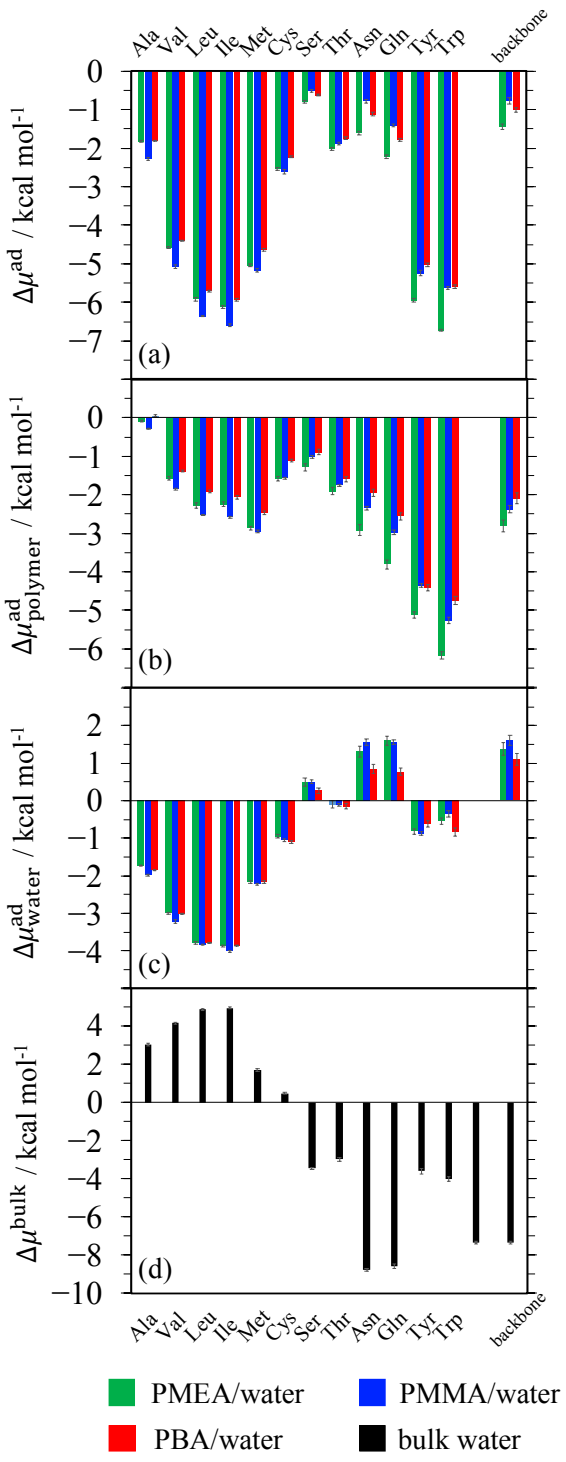

Figure 3: Adsorption free energies of amino-acid analogs: (a) the total value $\Delta\mu^{\mathrm{ad}}$, (b) the contribution from the polymer $\Delta\mu^{\mathrm{ad}}_{\mathrm{polymer}}$, and (c) the contribution from water $\Delta\mu^{\mathrm{ad}}_{\mathrm{water}}$. The solvation free energy in bulk water $\Delta\mu^{\mathrm{bulk}}$ is also shown in (d). The error (confidence interval) estimated from the 95% percentile with the bootstrap method in ref 70 is less than 0.3, 0.2, 0.2, and 0.1 kcal mol^{-1} for (a), (b), (c), and (d), respectively.

$\Delta\mu^{\mathrm{ad}}$ of the hydrophilic solute is seen to increase in magnitude when the hydrocarbon part of the solute becomes larger. The adsorption free energy is more favorable, indeed, for Thr than for Ser as well as for Gln than for Asn, and the large solutes of Tyr and Trp are strongly adsorbed

on the polymer/water interfaces. When the interfaces of PMEA, PMMA, and PBA are compared, $\Delta\mu^{\mathrm{ad}}$ of the hydrophilic solutes are always more favorable for PMEA than for the other two. PMEA has more polar moieties than PMMA and PBA, and the role of electrostatic interaction will be discussed later with respect to Figure 5. As listed in Table 1, the Met analog is obtained by replacing a methylene group of the Leu analog to a sulfur atom. The analog solute then becomes more hydrophilic, and $\Delta\mu^{\mathrm{ad}}$ is indeed more favorable to the water bulk for the Met analog than for Leu. The Ser analog changes into the Cys, on the other hand, by substituting the OH group with an SH. The hydrogen bonding is typically weaker for a thiol than an alcohol, and this tendency is reflected in Figure 3(a). The polymer/water interface is a less hydrophilic environment than the bulk water, and the Cys analog favors the interface more strongly than the Ser. Actually, the adsorption is weaker with more positive $\Delta\mu^{\mathrm{ad}}$ for a hydrophilic solute than for a hydrophobic one when they involve similar numbers of heavy (non-hydrogen) atoms. The hydrophilic moieties act to inhibit the adsorption onto the polymer/water interfaces. According to Figures 3(a) and 3(d), though, $\Delta\mu^{\mathrm{ad}}$ is not simply correlated to the extent of hydrophobicity/hydrophilicity of the solute expressed as the solvation free energy in the bulk water $\Delta\mu^{\mathrm{bulk}}$. The interaction with water alone is thus not enough to predict $\Delta\mu^{\mathrm{ad}}$, and the importance of the solute-polymer interactions is indicated.

Upon adsorption of a solute onto a polymer/water interface, the interactions with the polymer emerge and the interactions with water are (partially) lost. It is then insightful to separate the effects of the solute-polymer and solute-water interactions and discuss their roles in the adsorption free energy. The separated contributions of polymer and water are not observable, though, and there is a need for a model of free energy to conduct the separation. In the energy-representation formalism employed in the present work, the solvation free energy (free energy of transfer from the vacuum) $\Delta\mu$ is written formally as a sum of the partial contributions $\Delta\mu_i$ from species i (i is

either polymer or water). Accordingly, the adsorption free energy $\Delta\mu^{\mathrm{ad}}$ is written as

$$\Delta\mu^{\mathrm{ad}} = \Delta\mu^{\mathrm{ad}}_{\mathrm{polymer}} + \Delta\mu^{\mathrm{ad}}_{\mathrm{water}} \quad (2)$$

$$\Delta\mu^{\mathrm{ad}}_{\mathrm{polymer}} = \Delta\mu^{\mathrm{interface}}_{\mathrm{polymer}} \quad (3)$$

$$\Delta\mu^{\mathrm{ad}}_{\mathrm{water}} = \Delta\mu^{\mathrm{interface}}_{\mathrm{water}} - \Delta\mu^{\mathrm{bulk}} \quad (4)$$

where $\Delta\mu^{\mathrm{interface}}_{\mathrm{polymer}}$ and $\Delta\mu^{\mathrm{interface}}_{\mathrm{water}}$ are the contributions from the polymer and water to the solvation free energy at the polymer/water interface, respectively, and $\Delta\mu^{\mathrm{ad}}_{\mathrm{polymer}}$ and $\Delta\mu^{\mathrm{ad}}_{\mathrm{water}}$ are the polymer and water contributions to $\Delta\mu^{\mathrm{ad}}$, respectively. The separated roles of polymer and water in adsorption are discussed on the basis of eq 2.

Figures 3(b) and 3(c) show $\Delta\mu^{\mathrm{ad}}_{\mathrm{polymer}}$ and $\Delta\mu^{\mathrm{ad}}_{\mathrm{water}}$, respectively. $\Delta\mu^{\mathrm{ad}}_{\mathrm{polymer}}$ is favorable (negative) for the solutes and polymers examined (with a marginal exception of Ala on PBA), and accordingly, the interactions with the polymer contribute to the adsorption. It is further observed for each polymer that $\Delta\mu^{\mathrm{ad}}_{\mathrm{polymer}}$ increases in magnitude with the size of the analog solute. The polymer contribution to the adsorption free energy is more favorable for a solute with a larger number of heavy atoms. The correlation to the extent of hydrophobicity or hydrophilicity of the solute is not seen for $\Delta\mu^{\mathrm{ad}}_{\mathrm{polymer}}$, and as will be seen below with the analysis of the electrostatic, van der Waals, and excluded-volume components of the solute-polymer interactions, the dependence of $\Delta\mu^{\mathrm{ad}}_{\mathrm{polymer}}$ on the solute is governed by the van der Waals component. When PMEA, PMMA, and PBA are compared, $\Delta\mu^{\mathrm{ad}}_{\mathrm{polymer}}$ is most favorable with PMMA for the hydrophobic solutes and with PMEA for the hydrophilic. The ester groups in the polymers are hydrophilic, and the methyl groups located closely to ester facilitate the interactions of the hydrophobic solutes with the polymers. The ether oxygens in the polymers are additional sites to enhance the hydrophilicity of the polymers, and they contribute to the adsorptions of the hydrophilic solutes. $\Delta\mu^{\mathrm{ad}}_{\mathrm{water}}$ in Figure 3(c) exhibits a clear tendency with respect to the hydrophobicity or hydrophilicity of the solute. The hydrocarbon solutes are more favorable at the interface than in bulk water, and this is more so with the number of carbon atoms. The hydrophilic solutes are with marginal or unfavorable (positive)

$\Delta\mu^{\rm ad}_{\rm water}$. The interactions with water do not contribute to the adsorption, and $\Delta\mu^{\rm ad}_{\rm water}$ is particularly large for highly hydrophilic solutes such as Asn and Gln.

Correlation plots of $\Delta\mu^{\rm ad}$ with the polymer contribution $\Delta\mu^{\rm ad}_{\rm polymer}$ and the water contribution $\Delta\mu^{\rm ad}_{\rm water}$ are shown in Figures 4(a) and 4(b), respectively. Strong correlations are observed with both contributions over the hydrocarbon solutes of the Ala, Val, Leu, and Ile analogs. $\Delta\mu^{\rm ad}_{\rm polymer}$ and $\Delta\mu^{\rm ad}_{\rm water}$ are both favorable, meaning that the polymer and water act cooperatively for the adsorption. A correlation between $\Delta\mu^{\rm ad}_{\rm polymer}$ and the total $\Delta\mu^{\rm ad}$ is also seen over the hydrophilic analogs of Ser, Thr, Asn, Gln, Tyr, Trp, and backbone, while it is less evident than over the hydrophobic analogs. $\Delta\mu^{\rm ad}_{\rm polymer}$ of the hydrophilic solute increases in magnitude with the solute size, and the interaction with the polymer brings a larger solute more strongly to the interface. The correlation over the hydrophilic solutes is weak against the water contribution $\Delta\mu^{\rm ad}_{\rm water}$, on the other hand. $\Delta\mu^{\rm ad}_{\rm water}$ is smaller in magnitude than $\Delta\mu^{\rm ad}_{\rm polymer}$ for those solutes, and accordingly, the polymer contribution is decisive for the total $\Delta\mu^{\rm ad}$. For the solutes with similar values of the (total) $\Delta\mu^{\rm ad}$, $\Delta\mu^{\rm ad}_{\rm polymer}$ is more favorable (more negative) in the order of hydrophilic solutes $>$ sulfur-containing $>$ hydrophobic and $\Delta\mu^{\rm ad}_{\rm water}$ exhibits the opposite ordering. At a given extent of adsorption, the water contribution is more decisive for less polar solutes. Figure 4(c) is a correlation plot between $\Delta\mu^{\rm ad}_{\rm water}$ and $\Delta\mu^{\rm bulk}$. $\Delta\mu^{\rm ad}_{\rm water}$ refers to the loss of the water contribution upon transfer from the water bulk to the polymer/water interface, and $\Delta\mu^{\rm ad}_{\rm water}$ is more favorable when the free energy in the bulk $\Delta\mu^{\rm bulk}$ is more unfavorable (positive). The (negative) correlation in Figure 4(c) thus leads with Figure 4(b) to the (negative) correlation of the total free energy of adsorption $\Delta\mu^{\rm ad}$ with $\Delta\mu^{\rm bulk}$ for the hydrocarbon solutes. A more hydrophobic species is more favorably adsorbed onto the polymer/water interface. Figures 4(b) and 4(c) imply, on the other hand, that $\Delta\mu^{\rm ad}$ cannot be predicted from $\Delta\mu^{\rm bulk}$ for hydrophilic solutes. Figure 4(a) indicates instead that the polymer contribution needs to be taken into account to describe the extent of adsorption.

The extent of adsorption is determined by the cooperation and/or competition among a variety of intermolecular interactions, and it is of interest to assess the roles of interaction components such as electrostatic, van der Waals (dispersion), and excluded-volume in the adsorption free en-

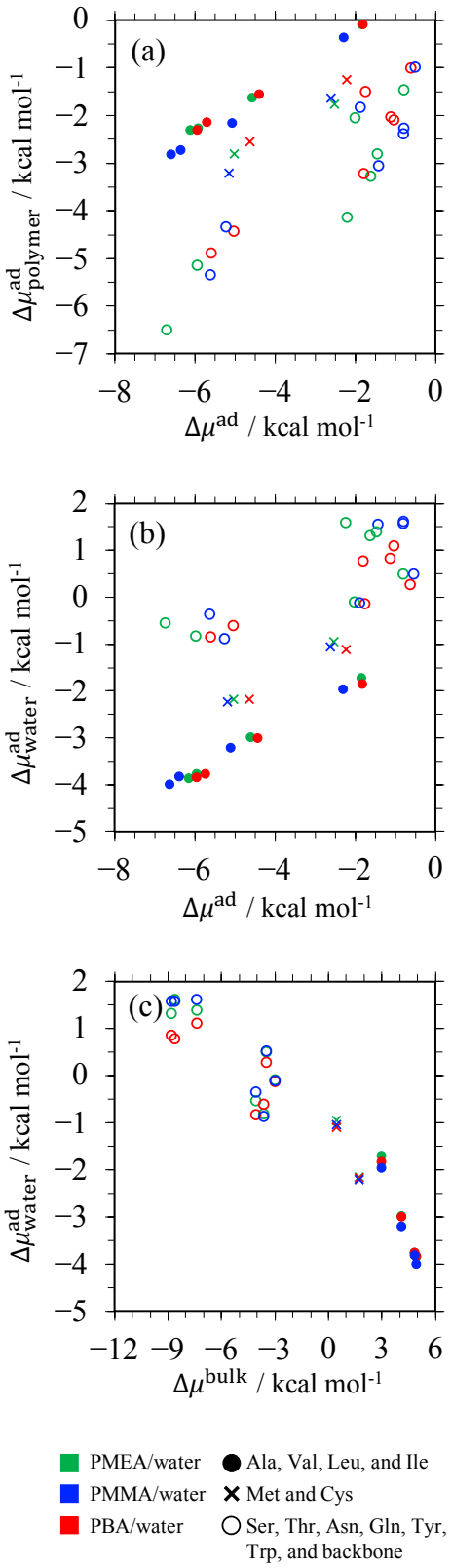

Figure 4: Correlation plots of the adsorption free energy $\Delta\mu^{ad}$ with (a) the polymer contribution $\Delta\mu^{ad}_{polymer}$ and (b) the water contribution $\Delta\mu^{ad}_{water}$, and (c) the plot between $\Delta\mu^{ad}_{water}$ and the solvation free energy $\Delta\mu^{bulk}$ in bulk water. The polymer and solute species are distinguished by the colors and forms of the symbols, respectively. The correlation coefficient is 0.99, 0.99, and 0.99 between $\Delta\mu^{ad}$ and $\Delta\mu^{ad}_{polymer}$, between $\Delta\mu^{ad}$ and $\Delta\mu^{ad}_{water}$, and between $\Delta\mu^{ad}_{water}$ and $\Delta\mu^{bulk}$, respectively, over the hydrocarbon solutes of the Ala, Val, Leu, and Ile analogs, and it is 0.84, 0.56, and 0.68 between $\Delta\mu^{ad}$ and $\Delta\mu^{ad}_{polymer}$, between $\Delta\mu^{ad}$ and $\Delta\mu^{ad}_{water}$, and between $\Delta\mu^{ad}_{water}$ and $\Delta\mu^{bulk}$, respectively, over Ser, Thr, Asn, Gln, Tyr, Trp, and backbone. The error (confidence interval) estimated from the 95% percentile with the bootstrap method in ref 70 is less than 0.3, 0.3, and 0.1 kcal mol^{-1} for the values on the abscissae of (a), (b), and (c), respectively, and 0.2, 0.2, and 0.2 kcal mol^{-1} for the values on the ordinates of (a), (b), and (c), respectively.

ergy. The electrostatic and van der Waals interactions are usually operative as attractive interaction components of the solute with the surrounding molecules. The former is more specific to the polarity or hydrogen-bonding ability of a molecule, and the latter reflects the molecular size. The excluded-volume effect corresponds to the free-energy penalty for displacing the polymer and/or water molecules from the region to be occupied by the solute. It is part of the repulsive components of the solute-polymer and solute-water interactions, and often plays decisive roles in structure formation of biomolecules.[71,72] In the energy-representation formalism, the contribution from species i (i refers either to the polymer or water) to the total solvation free energy $\Delta\mu$ is written as $\Delta\mu_i$ and is expressed as

$$\Delta\mu_i = u_{i,\mathrm{elec}} + u_{i,\mathrm{vdW}} + \int d\epsilon_i f(\epsilon_i) \tag{5}$$

where ϵ_i is the pair energy of the solute with solvent species i. It is supposed that the intermolecular interaction between the solute and species i consists of the electrostatic and van der Waals terms, and $u_{i,\mathrm{elec}}$ and $u_{i,\mathrm{vdW}}$ in eq 5 are the electrostatic and van der Waals components of the average sum of the interaction energy of the solute with species i in the "solution" system with the fully coupled solute; see METHODS section for the meaning of "solution". $f(\epsilon_i)$ takes into account the effects of structural reorganization of the molecules of species i due to introduction of the solute, and the excluded-volume component $\Delta\mu_{i,\mathrm{excl}}$ can be introduced by restricting the domain of integration in the third term of eq 5 to a high-energy region of $\epsilon_i > \epsilon^c$ as

$$\Delta\mu_{i,\mathrm{excl}} = \int_{\epsilon^c}^{\infty} d\epsilon_i f(\epsilon_i) \tag{6}$$

ϵ^c is the threshold for specifying the excluded-volume region. It was set to 10 kcal mol^{-1} in the present work by noting that $\epsilon_i > \epsilon^c$ was not sampled during the MD of the "solution" system. The choice of ϵ^c is rather arbitrary, in fact, and it is demonstrated in Figures S4-S6 that the following discussion concerning the excluded-volume component holds irrespective of the (reasonable) choice of the ϵ^c value.

The changes in the interaction components upon adsorption are introduced in parallel to eqs 2–

4. Let $u^{\mathrm{interface}}_{\mathrm{polymer,elec}}$ and $u^{\mathrm{interface}}_{\mathrm{water,elec}}$ be the electrostatic components of eq 5 in the interactions with the polymer and water of the solute located at the interface, respectively, and $u^{\mathrm{bulk}}_{\mathrm{elec}}$ be the one in bulk water. The total change in the electrostatic component upon adsorption $\Delta u^{\mathrm{ad}}_{\mathrm{elec}}$, the polymer contribution $\Delta u^{\mathrm{ad}}_{\mathrm{polymer,elec}}$, and the water contribution $\Delta u^{\mathrm{ad}}_{\mathrm{polymer,elec}}$ are then expressed as

$$\Delta u^{\mathrm{ad}}_{\mathrm{elec}} = \Delta u^{\mathrm{ad}}_{\mathrm{polymer,elec}} + \Delta u^{\mathrm{ad}}_{\mathrm{water,elec}} \quad (7)$$

$$\Delta u^{\mathrm{ad}}_{\mathrm{polymer,elec}} = u^{\mathrm{interface}}_{\mathrm{polymer,elec}} \quad (8)$$

$$\Delta u^{\mathrm{ad}}_{\mathrm{water,elec}} = u^{\mathrm{interface}}_{\mathrm{water,elec}} - u^{\mathrm{bulk}}_{\mathrm{elec}} \quad (9)$$

The total change $\Delta u^{\mathrm{ad}}_{\mathrm{vdW}}$, the polymer contribution $\Delta u^{\mathrm{ad}}_{\mathrm{polymer,vdW}}$, and the water contribution $\Delta u^{\mathrm{ad}}_{\mathrm{water,vdW}}$ in the van der Waals component are introduced with similar expressions as well as the corresponding excluded-volume components $\Delta \mu^{\mathrm{ad}}_{\mathrm{excl}}$, $\Delta \mu^{\mathrm{ad}}_{\mathrm{polymer,excl}}$, and $\Delta \mu^{\mathrm{ad}}_{\mathrm{water,excl}}$. We will elucidate below the roles of the electrostatic, van der Waals, excluded-volume components in the adsorption by examining their correlations to $\Delta \mu^{\mathrm{ad}}$ and the contributions from polymer and water. The solvent reorganization outside the excluded-volume domain ($\epsilon_i < \epsilon^c$) contributes to $\Delta \mu_i$ as the difference of the third term of eq 5 from $\Delta \mu_{i,\mathrm{excl}}$. The adsorption-induced change in the solvent-reorganization term of $\epsilon_i < \epsilon^c$ can be written similarly to eqs 7–9, and as shown in Figure S8 for each of the polymer and water contributions, it cancels partially the electrostatic and van der Waals components.

Figure 5 depicts the correlation plots for the (total) electrostatic component $\Delta u^{\mathrm{ad}}_{\mathrm{elec}}$ with the (total) free energy of adsorption $\Delta \mu^{\mathrm{ad}}$ and for the polymer and water contributions. $\Delta u^{\mathrm{ad}}_{\mathrm{elec}}$ is essentially zero for the hydrocarbon solutes of the Ala, Val, Leu, and Ile analogs. Its polymer contribution $\Delta u^{\mathrm{ad}}_{\mathrm{polymer,elec}}$ and the water contribution $\Delta u^{\mathrm{ad}}_{\mathrm{water,elec}}$ vanish in Figures 5(b) and 5(c), too, and the electrostatic interaction of the hydrocarbon solute does not play any roles in adsorption. The (total) $\Delta u^{\mathrm{ad}}_{\mathrm{elec}}$ is unfavorable (positive) for the other solutes. Although $\Delta u^{\mathrm{ad}}_{\mathrm{polymer,elec}}$ is favorable (negative), it is overturned by the contribution from water $\Delta u^{\mathrm{ad}}_{\mathrm{water,elec}}$. The correlation is weakly negative between $\Delta \mu^{\mathrm{ad}}$ and $\Delta u^{\mathrm{ad}}_{\mathrm{elec}}$ over the solutes other than the hydrocarbons,

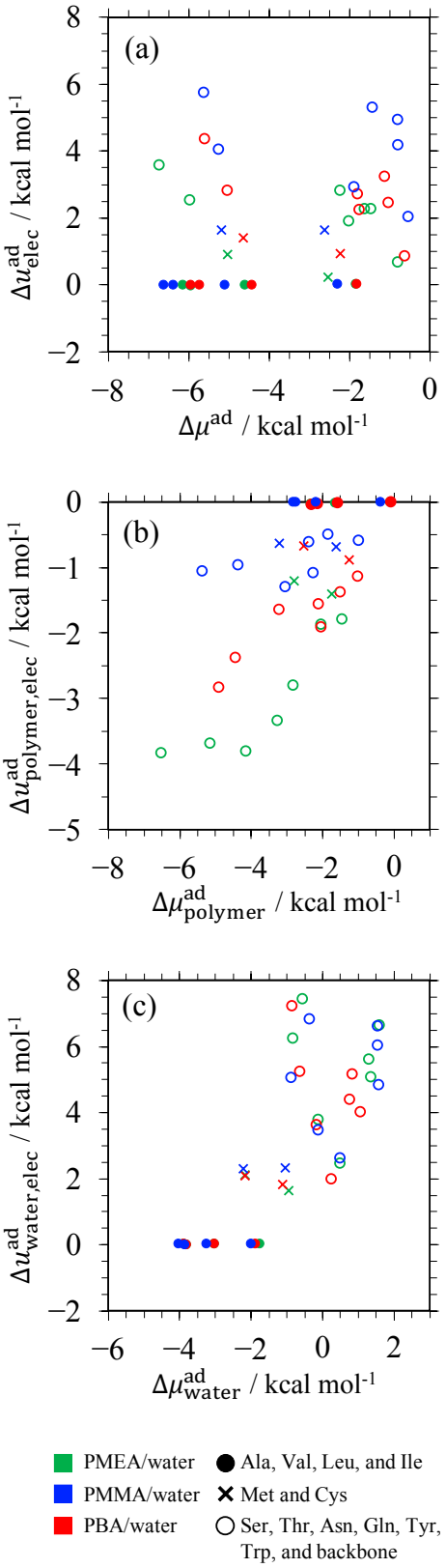

Figure 5: Correlation plots of (a) the total adsorption free energy $\Delta\mu^{\mathrm{ad}}$ with the total change in the electrostatic component upon adsorption $\Delta u^{\mathrm{ad}}_{\mathrm{elec}}$, (b) the polymer contribution $\Delta\mu^{\mathrm{ad}}_{\mathrm{polymer}}$ with $\Delta u^{\mathrm{ad}}_{\mathrm{polymer,elec}}$, and (c) water contribution $\Delta\mu^{\mathrm{ad}}_{\mathrm{water}}$ with $\Delta u^{\mathrm{ad}}_{\mathrm{water,elec}}$. The polymer and solute species are distinguished by the colors and forms of the symbols, respectively. The correlation coefficient is 0.17, 0.34, and 0.00 between $\Delta\mu^{\mathrm{ad}}$ and $\Delta u^{\mathrm{ad}}_{\mathrm{elec}}$, between $\Delta\mu^{\mathrm{ad}}_{\mathrm{polymer}}$ and $\Delta u^{\mathrm{ad}}_{\mathrm{polymer,elec}}$, and between $\Delta\mu^{\mathrm{ad}}_{\mathrm{water}}$ and $\Delta u^{\mathrm{ad}}_{\mathrm{water,elec}}$, respectively, over Ser, Thr, Asn, Gln, Tyr, Trp, and backbone. The error (confidence interval) estimated from the 95% percentile with the bootstrap method in ref 70 is less than 0.3, 0.2, and 0.2 kcal mol^{-1} for the values on the abscissae of (a), (b), and (c), respectively, and 0.9, 0.9, and 0.6 kcal mol^{-1} for the values on the ordinates of (a), (b), and (c), respectively. The data for the 3 polymer systems are plotted together in this figure, and the separated plots are provided in Figure S2.

furthermore, and the electrostatic component disfavors the adsorption due to the loss of electrostatic interactions with water. Figures 5 and S2 also show that when the solute is hydrophilic, $\Delta u^{\mathrm{ad}}_{\mathrm{polymer,elec}}$ is more favorable (more negative) on PMEA than on PMMA and PBA. It was seen in Figure 3 that the (total) free energy of adsorption $\Delta\mu^{\mathrm{ad}}$ is largest in magnitude on PMEA due to the polymer contribution $\Delta\mu^{\mathrm{ad}}_{\mathrm{polymer}}$, and this reflects the strong electrostatic interaction between the hydrophilic solute and PMEA.

Figure 6 provides the van der Waals components. It is observed that the total $\Delta u^{\mathrm{ad}}_{\mathrm{vdW}}$ is favorable for all the solutes examined and is well correlated to the (total) adsorption free energy $\Delta\mu^{\mathrm{ad}}$ separately over the hydrophobic solutes and over the hydrophilic and sulfur-containing solutes. The polymer contribution plotted in Figure 6(b) actually exhibits strong correlations between the van der Waals component $\Delta u^{\mathrm{ad}}_{\mathrm{polymer,vdW}}$ and the free energy $\Delta\mu^{\mathrm{ad}}_{\mathrm{polymer}}$, and in combination with Figure 4(a), the dependence of the adsorption propensity on the solute and polymer species is ranked by the van der Waals component in the polymer contribution both for the hydrophobic and hydrophilic solutes. The water contribution $\Delta u^{\mathrm{ad}}_{\mathrm{water,vdW}}$ in Figure 6(c) is unfavorable for all the combinations of solute and polymer and is anti-correlated to the corresponding free energy $\Delta\mu^{\mathrm{ad}}_{\mathrm{water}}$ only over the hydrocarbon solutes. $\Delta u^{\mathrm{ad}}_{\mathrm{water,vdW}}$ is still smaller in magnitude than $\Delta u^{\mathrm{ad}}_{\mathrm{polymer,vdW}}$ and is not decisive for the solute dependence of adsorption of the hydrophobic species. The van der Waals interaction is determined by the number of heavy (non-hydrogen) atoms around the solute. Figure S7 shows the number density of the heavy atoms in polymer around the solute at the polymer/water interface as well as the difference of the number density of water oxygen around the solute at the interface from that around the solute in bulk water. It is seen there that the accumulation of the polymer atoms around the solute at the interface is more in extents than the loss of water upon transfer of the solute from bulk to the interface, which corresponds to the energetic results in Figure 6 of $|\Delta u^{\mathrm{ad}}_{\mathrm{polymer,vdW}}| > \Delta u^{\mathrm{ad}}_{\mathrm{water,vdW}}$.

The excluded-volume component is shown in Figure 7. The total $\Delta\mu^{\mathrm{ad}}_{\mathrm{excl}}$ is negative for all the solutes, and the adsorption is favored by the excluded-volume component. It is also seen that $\Delta\mu^{\mathrm{ad}}_{\mathrm{polymer,excl}}$ in Figure 7(b) and $\Delta\mu^{\mathrm{ad}}_{\mathrm{water,excl}}$ in Figure 7(c) are unfavorable and favorable, respec-

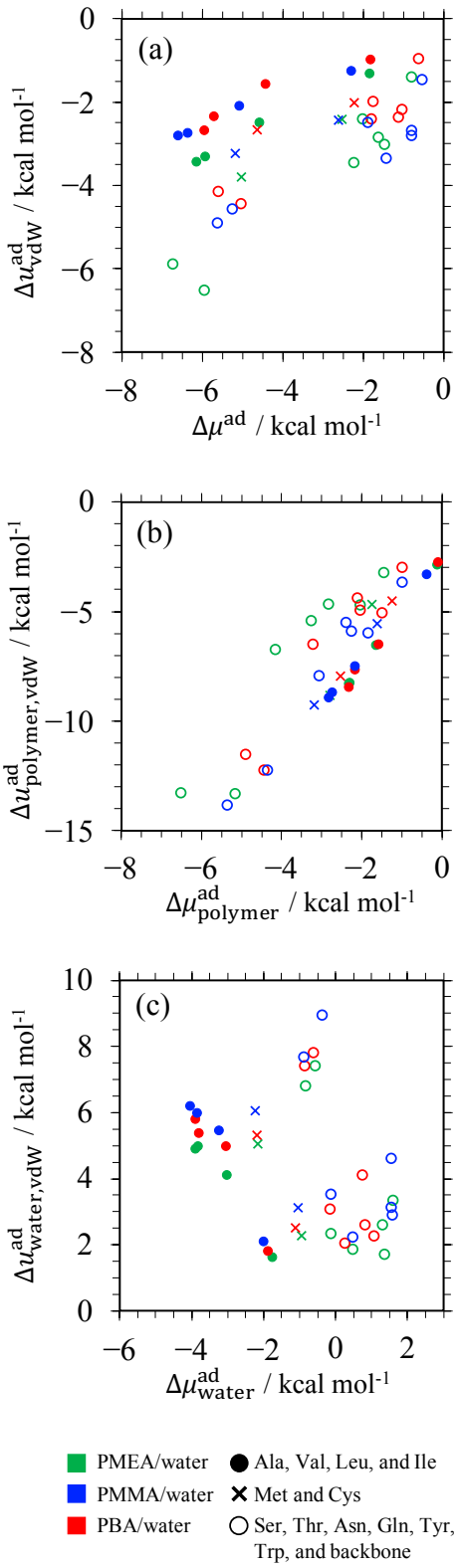

Figure 6: Correlation plots of (a) the total adsorption free energy $\Delta\mu^{\mathrm{ad}}$ with the total change in the van der Waals component upon adsorption $\Delta u^{\mathrm{ad}}_{\mathrm{vdW}}$, (b) the polymer contribution $\Delta\mu^{\mathrm{ad}}_{\mathrm{polymer}}$ with $\Delta u^{\mathrm{ad}}_{\mathrm{polymer,vdW}}$, and (c) water contribution $\Delta\mu^{\mathrm{ad}}_{\mathrm{water}}$ with $\Delta u^{\mathrm{ad}}_{\mathrm{water,vdW}}$. The polymer and solute species are distinguished by the colors and forms of the symbols, respectively. The correlation coefficient is 0.82, 0.98, and 0.90 between $\Delta\mu^{\mathrm{ad}}$ and $\Delta u^{\mathrm{ad}}_{\mathrm{vdW}}$, between $\Delta\mu^{\mathrm{ad}}_{\mathrm{polymer}}$ and $\Delta u^{\mathrm{ad}}_{\mathrm{polymer,vdW}}$, and between $\Delta\mu^{\mathrm{ad}}_{\mathrm{water}}$ and $\Delta u^{\mathrm{ad}}_{\mathrm{water,vdW}}$, respectively, over the hydrocarbon solutes of the Ala, Val, Leu, and Ile analogs, and it is 0.83, 0.90, and 0.40 between $\Delta\mu^{\mathrm{ad}}$ and $\Delta u^{\mathrm{ad}}_{\mathrm{vdW}}$, between $\Delta\mu^{\mathrm{ad}}_{\mathrm{polymer}}$ and $\Delta u^{\mathrm{ad}}_{\mathrm{polymer,vdW}}$, and between $\Delta\mu^{\mathrm{ad}}_{\mathrm{water}}$ and $\Delta u^{\mathrm{ad}}_{\mathrm{water,vdW}}$, respectively, over Ser, Thr, Asn, Gln, Tyr, Trp, and backbone. The error (confidence interval) estimated from the 95% percentile with the bootstrap method in ref 70 is less than 0.3, 0.2, and 0.2 kcal mol^{-1} for the values on the abscissae of (a), (b), and (c), respectively, and 1.1, 0.8, and 0.8 kcal mol^{-1} for the values on the ordinates of (a), (b), and (c), respectively. The data for the 3 polymer systems are plotted together in this figure, and the separated plots are provided in Figure S3.

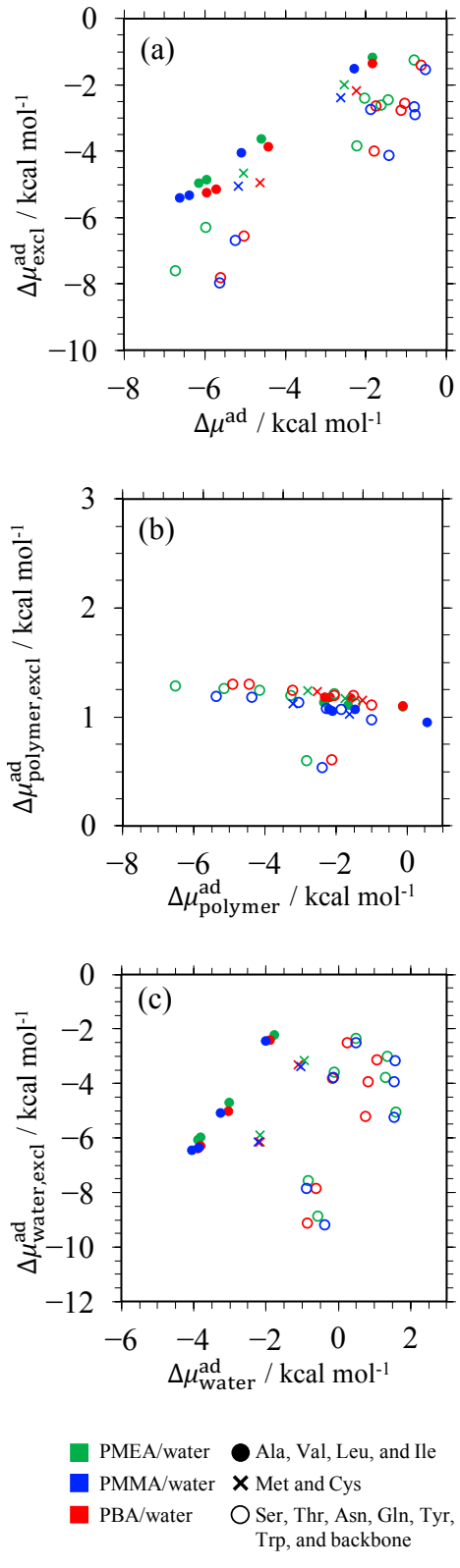

Figure 7: Correlation plots of (a) the total adsorption free energy $\Delta\mu^{ad}$ with the total change in the excluded-volume component upon adsorption $\Delta\mu^{ad}_{excl}$, (b) the polymer contribution $\Delta\mu^{ad}_{polymer}$ with $\Delta\mu^{ad}_{polymer,excl}$, and (c) water contribution $\Delta\mu^{ad}_{water}$ with $\Delta\mu^{ad}_{water,excl}$. The polymer and solute species are distinguished by the colors and forms of the symbols, respectively. The correlation coefficient is 0.98, 0.11, and 0.99 between $\Delta\mu^{ad}$ and $\Delta\mu^{ad}_{excl}$, between $\Delta\mu^{ad}_{polymer}$ and $\Delta\mu^{ad}_{polymer,excl}$, and between $\Delta\mu^{ad}_{water}$ and $\Delta\mu^{ad}_{water,excl}$, respectively, over the hydrocarbon solutes of the Ala, Val, Leu, and Ile analogs, and it is 0.91, 0.17, and 0.42 between $\Delta\mu^{ad}$ and $\Delta\mu^{ad}_{excl}$, between $\Delta\mu^{ad}_{polymer}$ and $\Delta\mu^{ad}_{polymer,excl}$, and between $\Delta\mu^{ad}_{water}$ and $\Delta\mu^{ad}_{water,excl}$, respectively, over Ser, Thr, Asn, Gln, Tyr, Trp, and backbone. The error (confidence interval) estimated from the 95% percentile with the bootstrap method in ref 70 is less than 0.3, 0.2, and 0.2 kcal mol^{-1} for the values on the abscissae of (a), (b), and (c), respectively, and 0.6, 0.6, and 0.9 kcal mol^{-1} for the values on the ordinates of (a), (b), and (c), respectively. The data for the 3 polymer systems are plotted together in this figure, and the separated plots are provided in Figure S4.

tively. When the solute is brought from bulk water to the polymer/water interface, the excluded-volume effect emerges against the polymer and is partially lost against water. Although the signs of the polymer and water contributions for the excluded-volume component are opposite to those for the electrostatic and van der Waals components in Figures 5 and 6, all of the three interaction components behave in parallel in the sense that the interaction is gained with the polymer and is lost with water. The polymer contribution in Figure 7(b) is actually small, and the excluded-volume component drives the adsorption due to the water contribution in Figure 7(c). It is observed in Figures 7 and S4, in fact, that the magnitudes of $\Delta\mu^{\rm ad}_{\rm excl}$ and $\Delta\mu^{\rm ad}_{\rm water,excl}$ correspond to the solute size separately over the hydrophobic and hydrophilic solutes. At adsorption, the excluded-volume effect operates more favorably for a larger solute through the water contribution over each class of solutes. The connection to the number of solvent molecules to be displaced from the region occupied by the solute is further addressed in Supporting Information with respect to Figure S9. $\Delta\mu^{\rm ad}_{\rm polymer,excl}$ does not vary strongly with the solute and polymer species. The polymer contribution is not distinguished by the excluded-volume component, whereas $\Delta\mu^{\rm ad}_{\rm polymer,excl}$ is smaller for the backbone analog than for the other solutes that have similar numbers of heavy (non-hydrogen) atoms. This reflects the cyclic structure of the backbone solute. The volume is smaller for a cyclic molecule than for a linear one even when the numbers of atoms involved are the same. A similar trend is not observed for the total $\Delta\mu^{\rm ad}_{\rm excl}$ and the water contribution $\Delta\mu^{\rm ad}_{\rm water,excl}$, though, since the contribution in the bulk water is subtracted.

It is thus revealed from Figures 4-7 that among the electrostatic, van der Waals, and excluded-volume components, the polymer contribution in the van der Waals component plays the key role in determining the ranking of the adsorption propensity separately over the hydrophobic and hydrophilic solutes. The adsorption is disfavored by the electrostatic component, on the other hand, and is driven by the excluded-volume component through the water contribution.

CONCLUSION

All-atom analyses were conducted for the adsorption of a variety of solute molecules onto the interfaces of PMEA, PMMA, and PBA with water. It was found for the polymer/water interface that water penetrates to the polymer region, with the extent being smaller for the hydrophobic PBA. The free energy of adsorption was computed by the energy-representation method. The adsorption free energy was favorable (negative) for all the combination of solute and polymer, and the adsorption was strongest on PMMA for the hydrophobic solutes and on PMEA for the hydrophilic ones. The adsorption free energy was then decomposed into the contributions from polymer and water. The polymer contribution was seen to be more favorable for larger solutes, while a clear correlation with the hydrophobicity or hydrophilicity was observed for the water contribution. The extent of adsorption may be addressed from the solvation free energy in bulk water only for hydrophobic solutes. The roles of the intermolecular interaction components such as electrostatic, van der Waals, and excluded-volume in the adsorption energetics were further examined within the framework of the energy-representation formalism. It was shown that the extent of adsorption can be ranked by the van der Waals component in the polymer contribution separately over the hydrophilic and hydrophobic solutes, with the excluded-volume effect driving the adsorption due to the water contribution. The electrostatic component was seen to disfavor the adsorption and was not influential to determine the solute dependence of the adsorption capacity.

The adsorption capacity is an important property of a polymer in medical and industrial applications. This property is determined by the balance of interactions among the adsorbate, polymer, and water. The present work was conducted to systematically analyze the adsorption energetics for a wide variety of adsorbate solutes, through all-atom MD simulation and free-energy calculations that were shown to be well feasible. Peptide or protein molecules appearing in applications to medical devices or separation membranes are still larger than amino-acid analogs treated in this work and may consist both of hydrophobic and hydrophilic moieties. Extension to peptides of a few residues will thus be of interest, as well as to polymer interfaces with varied extents of hydrophobicity and hydrophilicity.

APPENDIX A: Determination of the atomic partial charges

This Appendix describes the scheme to determine the atomic partial charges on the polymers and amino-acid analogs. For each of them, a quantum-chemical calculation with B3LYP and the 6-31G(d) basis set was carried out with Gaussian 09.[73] In the case of the polymer molecules, the degree of polymerization in Figure 1 was set to $N = 5$ and the all-*trans* conformation was adopted as the initial configuration. Through the geometry optimization, the atomic partial charges were obtained using the restrained electrostatic potential (RESP) procedure.[53] The charges used in MD were determined with

$$q_i^{\mathrm{QM}} - \frac{1}{M}\sum_{i=1}^{M} q_i^{\mathrm{QM}} \tag{10}$$

where q_i^{QM} is the charge on the ith atom. Eq 10 is a scheme of neutralization for a unit consisting of M atoms. This unit is set to the central monomer (3rd both from the left and right in Figure 1 at $N = 5$) for the polymers and to the whole molecule for the amino-acid analogs. In the polymers, the atomic charges thus determined were used for all of the monomers except for the terminals. The atomic charges in the terminal monomer were modified from those in the inner monomers, given that a hydrogen was added as depicted in Figure 1. The terminal monomer was made neutral by employing the same charges as in the inner monomer for the atoms other than the terminal H atoms and assigning the equal charges to the equivalent H.

Supporting Information Available

Figure S1: Density profiles of the polymer/water systems at $N = 40$. Figure S2: Electrostatic components plotted separately for the 3 polymers. Figure S3: van der Waals components plotted separately for the 3 polymers. Figure S4: Excluded-volume components at ϵ^c = 10 kcal mol^{-1} plotted separately for the 3 polymers. Figure S5: Excluded-volume components at ϵ^c = 5 kcal mol^{-1} plotted separately for the 3 polymers. Figure S6: Excluded-volume components at ϵ^c = 20 kcal mol^{-1} plotted separately for the 3 polymers. Figure S7: Distributions of the heavy atoms in

polymer and water around the solute. Figure S8: Solvent-reorganization term outside the excluded-volume domain plotted against the sum of the electrostatic and van der Waals components. Figure S9: Number of displaced solvent molecules upon adsorption plotted against the excluded-volume component.

Acknowledgement

This work is supported by the Grant-in-Aid for Scientific Research (No. JP19H04206) from the Japan Society for the Promotion of Science and by the Fugaku Supercomputer Project (No. JPMXP1020200308) and the Elements Strategy Initiative for Catalysts and Batteries (No. JPMXP0112101003) from the Ministry of Education, Culture, Sports, Science, and Technology. The simulations were conducted partly using ITO at Kyushu University, OCTOPUS at Osaka University, Grand Chariot at Hokkaido University, and Fugaku at RIKEN Advanced Institute for Computational Science through the HPCI System Research Project (Project IDs: hp200120, hp210176, and hp220176)

References

(1) Calucci, L.; Forte, C.; Ranucci, E. Water/polymer interactions in a poly(amidoamine) hydrogel studied by NMR spectroscopy. *Biomacromolecules* **2007**, *8*, 2936–2942.

(2) Zhao, Z. J.; Wang, Q.; Zhang, L.; Wu, T. Structured water and water-polymer interactions in hydrogels of molecularly imprinted polymers. *J. Phys. Chem. B* **2008**, *112*, 7515–7521.

(3) Kamei, D.; Ajiro, H.; Akashi, M. Morphological changes of isotactic poly(methyl methacrylate) thin films via self-organization and stereocomplex formation. *Polym. J.* **2010**, *42*, 131–137.

(4) Black, S. B.; Chang, Y.; Bae, C.; Hickner, M. A. FTIR characterization of water-polymer interactions in superacid polymers. *J. Phys. Chem. B* **2013**, *117*, 16266–16274.

(5) Zhu, H.; Huinink, H. P.; Adan, O. C.; Kopinga, K. NMR study of the microstructures and water-polymer interactions in cross-linked polyurethane coatings. *Macromolecules* **2013**, *46*, 6124–6131.

(6) Li, Z.; Yuan, F.; Fichthorn, K. A.; Milner, S. T.; Larson, R. G. Molecular view of polymer/water interfaces in latex paint. *Macromolecules* **2014**, *47*, 6441–6452.

(7) Tavagnacco, L.; Chiessi, E.; Zanatta, M.; Orecchini, A.; Zaccarelli, E. Water-polymer coupling induces a dynamical transition in microgels. *J. Phys. Chem. Lett.* **2019**, *10*, 870–876.

(8) Yasoshima, N.; Fukuoka, M.; Kitano, H.; Kagaya, S.; Ishiyama, T.; Gemmei-Ide, M. Diffusion-Controlled Recrystallization of Water Sorbed into Poly(meth)acrylates Revealed by Variable-Temperature Mid-Infrared Spectroscopy and Molecular Dynamics Simulation. *J. Phys. Chem. B* **2017**, *121*, 5133–5141.

(9) Yasoshima, N.; Ishiyama, T.; Gemmei-Ide, M.; Matubayasi, N. Molecular Structure and Vibrational Spectra of Water Molecules Sorbed in Poly(2-methoxyethylacrylate) Revealed by Molecular Dynamics Simulation. *J. Phys. Chem. B* **2021**, *125*, 12095–12103.

(10) Tanaka, M.; Motomura, T.; Kawada, M.; Anzai, T.; Yuu Kasori,; Shiroya, T.; Shimura, K.; Onishi, M.; Akira Mochizuki, Blood compatible aspects of poly(2-methoxyethylacrylate) (PMEA)-relationship between protein adsorption and platelet adhesion on PMEA surface. *Biomaterials* **2000**, *21*, 1471–1481.

(11) Morita, S.; Tanaka, M.; Ozaki, Y. Time-resolved in situ ATR-IR observations of the process of sorption of water into a poly(2-methoxyethyl acrylate) film. *Langmuir* **2007**, *23*, 3750–3761.

(12) Tanaka, M.; Mochizuki, A. Effect of water structure on blood compatibility– thermal analysis of water in poly(meth)acrylate. *J. Biomed. Mater. Res. A* **2004**, *68A*, 684–695.

(13) Wolfenden, R.; Andersson, L.; Cullis, P. M.; Southgate, C. C. B. Affinities of amino acid side-chains for solvent water. *Biochemistry* **1981**, *20*, 849–855.

(14) Frenkel, D.; Smit, B. *Understanding Molecular Simulation From Algorithms to Applications*; 2nd ed.; Academic Press: London, U.K., 2002.

(15) Allen, M. P.; Tildesley, D. J. *Computer Simulation of Liquids.*; 2nd ed.; Oxford University Press: New York, U.K., 2017.

(16) Matubayasi, N.; Nakahara, M. Theory of solutions in the energetic representation. I. Formulation. *J. Chem. Phys.* **2000**, *113*, 6070.

(17) Matubayasi, N.; Nakahara, M. Theory of solutions in the energy representation. II. Functional for the chemical potential. *J. Chem. Phys.* **2002**, *117*, 3605–3616.

(18) Matubayasi, N.; Nakahara, M. Erratum: Theory of solutions in the energy representation II. Functional for the chemical potential (J. Chem. Phys. (2002) 117 (3605)). *J. Chem. Phys.* **2003**, *118*, 2446.

(19) Matubayasi, N.; Nakahara, M. Theory of solutions in the energy representation. III. Treatment of the molecular flexibility. *J. Chem. Phys.* **2003**, *119*, 9686–9702.

(20) Åqvist, J.; Medina, C.; Samuelsson, J.-E. A new method for predicting binding affinity in computer-aided drug design. *Protein Eng. Des. Sel.* **1994**, *7*, 385–391.

(21) Carlson, H. A.; Jorgensen, W. L. An Extended Linear Response Method for Determining Free Energies of Hydration. *J. Phys. Chem.* **1995**, *99*, 10667–10673.

(22) Kast, S. M. Combinations of simulation and integral equation theory. *Phys. Chem. Chem. Phys.* **2001**, *3*, 5087–5092.

(23) Hirata, F. *Molecular Theory of Solvation*; Kluwer Academic Publishers: Dordrecht, Netherlands, 2003.

(24) Galván, I. F.; Sánchez, M. L.; Martín, M. E.; Olivares del Valle, F. J.; Aguilar, M. A. Geometry optimization of molecules in solution: Joint use of the mean field approximation and the free-energy gradient method. *J. Chem. Phys.* **2003**, *118*, 255–263.

(25) Freedman, H.; Truong, T. N. Coupled reference interaction site model/simulation approach for thermochemistry of solvation: Theory and prospects. *J. Chem. Phys.* **2004**, *121*, 2187–2198.

(26) Chuev, G. N.; Fedorov, M. V.; Crain, J. Improved estimates for hydration free energy obtained by the reference interaction site model. *Chem. Phys. Lett.* **2007**, *448*, 198–202.

(27) Kokubo, H.; Hu, C. Y.; Pettitt, B. M. Peptide conformational preferences in osmolyte solutions: Transfer free energies of decaalanine. *J. Am. Chem. Soc.* **2011**, *133*, 1849–1858.

(28) Frolov, A. I.; Ratkova, E. L.; Palmer, D. S.; Fedorov, M. V. Hydration thermodynamics using the reference interaction site model: Speed or accuracy? *J. Phys. Chem. B* **2011**, *115*, 6011–6022.

(29) Weber, V.; Asthagiri, D. Regularizing binding energy distributions and the hydration free energy of protein cytochrome C from all-atom simulations. *J. Chem. Theory Comput.* **2012**, *8*, 3409–3415.

(30) Sergiievskyi, V.; Jeanmairet, G.; Levesque, M.; Borgis, D. Solvation free-energy pressure corrections in the three dimensional reference interaction site model. *J. Chem. Phys.* **2015**, *143*, 184116.

(31) Ratkova, E. L.; Palmer, D. S.; Fedorov, M. V. Solvation Thermodynamics of Organic Molecules by the Molecular Integral Equation Theory: Approaching Chemical Accuracy. *Chem. Rev.* **2015**, *115*, 6312–6356.

(32) Persson, R. A.; Pattni, V.; Singh, A.; Kast, S. M.; Heyden, M. Signatures of Solvation Thermodynamics in Spectra of Intermolecular Vibrations. *J. Chem. Theory Comput.* **2017**, *13*, 4467–4481.

(33) Luukkonen, S.; Levesque, M.; Belloni, L.; Borgis, D. Hydration free energies and solvation

structures with molecular density functional theory in the hypernetted chain approximation. *J. Chem. Phys.* **2020**, *152*, 064110.

(34) Matubayasi, N.; Liang, K. K.; Nakahara, M. Free-energy analysis of solubilization in micelle. *J. Chem. Phys.* **2006**, *124*, 154908.

(35) Matubayasi, N.; Shinoda, W.; Nakahara, M. Free-energy analysis of the molecular binding into lipid membrane with the method of energy representation. *J. Chem. Phys.* **2008**, *128*, 195107.

(36) Karino, Y.; Fedorov, M. V.; Matubayasi, N. End-point calculation of solvation free energy of amino-acid analogs by molecular theories of solution. *Chem. Phys. Lett.* **2010**, *496*, 351–355.

(37) Takahashi, H.; Maruyama, K.; Karino, Y.; Morita, A.; Nakano, M.; Jungwirth, P.; Matubayasi, N. Energetic origin of proton affinity to the air/water interface. *J. Phys. Chem. B* **2011**, *115*, 4745–4751.

(38) Kawakami, T.; Shigemoto, I.; Matubayasi, N. Free-energy analysis of water affinity in polymer studied by atomistic molecular simulation combined with the theory of solutions in the energy representation Free-energy analysis of water affinity in polymer studied by atomistic molecular simulation comb. *J. Chem. Phys.* **2012**, *137*, 234903.

(39) Karino, Y.; Matubayasi, N. Interaction-component analysis of the urea effect on amino acid analogs. *Phys. Chem. Chem. Phys.* **2013**, *15*, 4377–4391.

(40) Sakuraba, S.; Matubayasi, N. ERmod: Fast and versatile computation software for solvation free energy with approximate theory of solutions. *J. Comput. Chem.* **2014**, *35*, 1592–1608.

(41) Date, A.; Ishizuka, R.; Matubayasi, N. Energetics of nonpolar and polar compounds in cationic, anionic, and nonionic micelles studied by all-atom molecular dynamics simulation combined with a theory of solutions. *Phys. Chem. Chem. Phys.* **2016**, *18*, 13223–13231.

(42) Yamamoto, N.; Nakakuki, I.; Matubayasi, N. Free-energy analysis of physisorption on solid-liquid interface with the solution theory in the energy representation. *J. Chem. Phys.* **2018**, *149*, 014504.

(43) Kawakami, T.; Shigemoto, I.; Matubayasi, N. Structure and permeability of ionomers studied by atomistic molecular simulation combined with the theory of solutions in the energy representation. *J. Chem. Phys.* **2018**, *148*, 214903.

(44) Matubayasi, N. Energy-representation theory of solutions: Its formulation and application to soft, molecular aggregates. *Bull. Chem. Soc. Jpn.* **2019**, *92*, 1910–1927.

(45) Mizuguchi, T.; Matubayasi, N. Free-Energy Analysis of Peptide Binding in Lipid Membrane Using All-Atom Molecular Dynamics Simulation Combined with Theory of Solutions. *J. Phys. Chem. B* **2018**, *122*, 3219–3229.

(46) Yamada, K.; Matubayasi, N. Chain-Increment Method for Free-Energy Computation of a Polymer with All-Atom Molecular Simulations. *Macromolecules* **2020**, *53*, 775–788.

(47) See http://www.j–octa.com for J–OCTA. It is a simulation software for multi–scale modeling of polymeric material.

(48) Shirts, M. R.; Pitera, J. W.; Swope, W. C.; Pande, V. S. Extremely precise free energy calculations of amino acid side chain analogs: Comparison of common molecular mechanics force fields for proteins. *J. Chem. Phys.* **2003**, *119*, 5740–5761.

(49) Auton, M.; Bolen, D. W. Additive Transfer Free Energies of the Peptide Backbone Unit That Are Independent of the Model Compound and the Choice of Concentration Scale. *Biochemistry* **2004**, *43*, 1329–1342.

(50) Auton, M.; Bolen, D. W. Predicting the energetics of osmolyte-induced protein folding/unfolding. *Proc. Natl. Acad. Sci. USA* **2005**, *102*, 15065–15068.

(51) Wang, J. M.; Wolf, R. M.; Caldwell, J. W.; Kollman, P. A.; Case, D. A. Development and testing of a general amber force field. *J. Comput. Chem.* **2004**, *25*, 1157–1174.

(52) Jorgensen, W. L.; Chandrasekhar, J.; Madura, J. D.; Impey, R. W.; Klein, M. L. Comparison of simple potential functions for simulating liquid water. *J. Chem. Phys.* **1983**, *79*, 926–935.

(53) Bayly, C. I.; Cieplak, P.; Cornell, W.; Kollman, P. A. A well-behaved electrostatic potential based method using charge restraints for deriving atomic charges: the RESP model. *J. Phys. Chem.* **1993**, *97*, 10269–10280.

(54) Abraham, M. J.; Murtola, T.; Schulz, R.; Páll, S.; Smith, J. C.; Hess, B.; Lindah, E. Gromacs: High performance molecular simulations through multi-level parallelism from laptops to supercomputers. *SoftwareX* **2015**, *1-2*, 19–25.

(55) Darden, T.; York, D.; Pedersen, L. Particle mesh Ewald: An $N\cdot\log(N)$ method for Ewald sums in large systems. *J. Chem. Phys.* **1993**, *98*, 10089.

(56) Essmann, U.; Perera, L.; Berkowitz, M. L.; Darden, T.; Lee, H.; Pedersen, L. G. A smooth particle mesh Ewald method. *J. Chem. Phys.* **1995**, *103*, 8577–8593.

(57) Caleman, C.; van Maaren, P. J.; Hong, M.; Hub, J. S.; Costa, L. T.; van der Spoel, D. Force Field Benchmark of Organic Liquids: Density, Enthalpy of Vaporization, Heat Capacities, Surface Tension, Isothermal Compressibility, Volumetric Expansion Coefficient, and Dielectric Constant. *J. Chem. Theory Comput.* **2012**, *8*, 61–74.

(58) Martinez, L.; Andrade, R.; Birgin, E. G.; Martinez, J. M. PACKMOL: A Package for Building Initial Configurations for Molecular Dynamics Simulations. *J. Comput. Chem.* **2009**, *30*, 2157–2164.

(59) van Gunsteren, W.; Berendsen, H. A Leap-Frog Algorithm for Stochastic Dynamics. *Mol. Simul.* **1988**, *1*, 173–185.

(60) Goga, N.; Rzepiela, A. J.; de Vries, A. H.; Marrink, S. J.; Berendsen, H. J. C. Efficient Algorithms for Langevin and DPD Dynamics. *J. Chem. Theory Comput.* **2012**, *8*, 3637–3649.

(61) Parrinello, M.; Rahman, A. Polymorphic transitions in single crystals: A new molecular dynamics method. *J. Appl. Phys.* **1981**, *52*, 7182–7190.

(62) Hess, B.; Bekker, H.; Berendsen, H. J. C.; Fraaije, J. G. E. M. LINCS: A linear constraint solver for molecular simulations. *J. Comput. Chem.* **1997**, *18*, 1463–1472.

(63) Miyamoto, S.; Kollman, P. A. Settle: An analytical version of the SHAKE and RATTLE algorithm for rigid water models. *J. Comput. Chem.* **1992**, *13*, 952–962.

(64) Theodorakis, P. E.; Fytas, N. G. A study for the static properties of symmetric linear multi-block copolymers under poor solvent conditions. *J. Chem. Phys.* **2012**, *136*, 094902.

(65) Fu, Y.; Liao, L.; Lan, Y.; Yang, L.; Mei, L.; Liu, Y.; Hu, S. Molecular dynamics and mesoscopic dynamics simulations for prediction of miscibility in polypropylene/polyamide-11 blends. *J. Mol. Struct.* **2012**, *1012*, 113–118.

(66) Mokshin, A. V.; Galimzyanov, B. N.; Barrat, J. L. Extension of classical nucleation theory for uniformly sheared systems. *Phys. Rev. E* **2013**, *87*, 062307.

(67) Knapp, B.; Ospina, L.; Deane, C. M. Avoiding False Positive Conclusions in Molecular Simulation: The Importance of Replicas. *J. Chem. Theory Comput.* **2018**, *14*, 6127–6138.

(68) Gartner, T. E.; Jayaraman, A. Modeling and Simulations of Polymers: A Roadmap. *Macromolecules* **2019**, *52*, 755–786.

(69) Kishinaka, S.; Morita, A.; Ishiyama, T. Molecular structure and vibrational spectra at water/poly(2-methoxyethylacrylate) and water/poly(methyl methacrylate) interfaces: A molecular dynamics simulation study. *J. Chem. Phys.* **2019**, *150*, 044707.

(70) Kojima, H.; Handa, K.; Yamada, K.; Matubayasi, N. Water Dissolved in a Variety of Polymers Studied by Molecular Dynamics Simulation and a Theory of Solutions. *J. Phys. Chem. B* **2021**, *125*, 9357–9371.

(71) Kinoshita, M. A new theoretical approach to biological self-assembly. *BioPhys. Rev.* **2013**, *5*, 283–293.

(72) Kinoshita, M. Roles of translational motion of water molecules in sustaining life. *Front. Biosci.* **2009**, *14*, 3419–3454.

(73) Frisch, M. J.; Trucks, G. W.; Schlegel, H. B.; Scuseria, G. E.; Robb, M. A.; Cheeseman, J. R.; Scalmani, G.; Barone, V.; B., M.; Petersson, G. A. Gaussian 09, revision A.02; Gaussian, Inc.: Wallingford CT, 2009.

Graphical TOC Entry

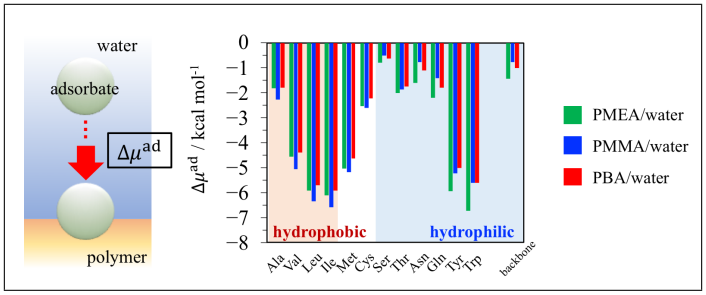

TOC Graphic